Analytical modeling of wave generation by the Borehole Orbital Vibrator Source

Seiji Nakagawa and Thomas M. Daley

Center for Computational Seismology (CCS), Earth Sciences Division
E.O. Lawrence Berkeley National Laboratory, Berkeley CA 94720

ABSTRACT

The orbital vibrator source (a fluid-coupled shear wave source) has many unique properties that are useful for cross-well, single-well, and borehole-to-surface imaging of both P-(compressional) and S- (shear) wave velocities of reservoir rocks. To this day, however, no standard models for this source have been established, and the mechanism of wave generation and the characteristics of wave field around the source are not well understood yet. In this article, we develop both two and three-dimensional analytical models of the orbital vibrator source, which allow us to examine the source characteristics such as radiation patterns, frequency-dependence of the wave energy, and guided-wave generation. These models are developed in the frequency-wavenumber domain using the partial wave expansion of the wavefield within and outside the borehole. The results show that the developed models successfully reproduce many characteristics of orbital vibrator source that have been observed in the field, including formation property-dependent vibrator amplitudes, uniform isotropic shear wave radiation pattern, and small tube-wave generation.

INTRODUCTION

The orbital vibrator source (OVS) was originally developed by Conoco, Inc. in the 1980s to generate S waves from a fluid-filled borehole without the direct mechanical coupling of borehole seismic sources to the borehole wall. Cole (1997) summarized the historical background of the orbital source. There are two types of the borehole orbital vibrator sources: one is a mechanical source (Figure 1a), and the other is a solid-state, piezoelectric source (Figure 1b). Currently, only the mechanical source is used for field applications, and we will primarily discuss the wave generation mechanism of the mechanical source.

(a) Mechanical OVS (b) Piezoelectric OVS

FIG. 1 Bohole orbital vibrator sources. Currently, only the mechanical OVS (left) is used in the field. The piezoelectric OVS (right) generates waves by sequentially firing an array of piezoelectric elements and, potentially, can generates waves at much higher frequencies.

The mechanical source consists of an eccentric mass spinning around the source axis, encased in a cylindrical housing that is suspended in the borehole fluid. The centrifugal force induced by the rotation of the mass moves the whole source in the radial directions of the borehole, introducing the compression of the fluid on one side and tension on the other side of the source (Figure 2). On the borehole wall, a part of this compressional motion is converted into shear motions that are, in principle, both vertically (parallel to the borehole, *Sv*) and horizontally (perpendicular to the borehole, *Sh*) polarized. Because of this wave-generating mechanism, the resulting waves have the same primary frequency as the spin frequency of the source. The currently used mechanical source can generate waves with useful amplitudes at frequencies approximately between 70 Hz and 400 Hz. The same wave generating effect can be produced using a phased, circular allay of piezoelectric sources around the borehole axis, which can generate waves above 4 kilohertz (e.g., Cole, 1997).

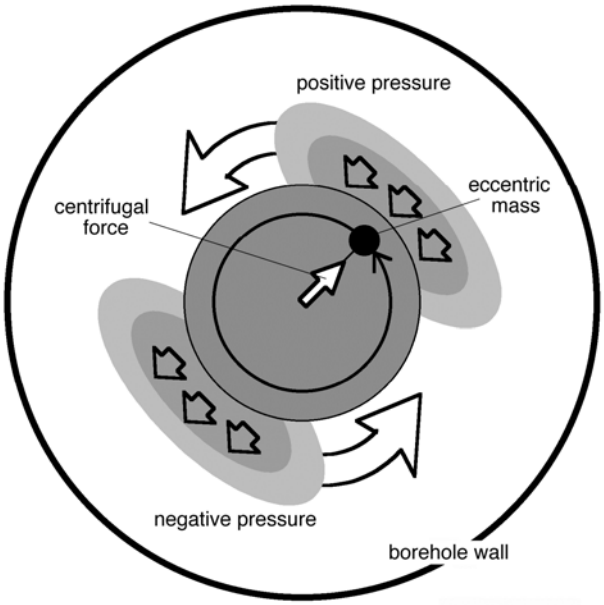

FIG. 2 A cross section of a mechanical OVS within a borehole. The rotational motion of the source induced by a spinning eccentric mass generates rotating positive and negative pressure perturbations within the fluid.

An OVS has many unique and attractive properties as a fluid-coupled, borehole *S*-wave source. For example, unlike conventional borehole sources that generate *Sv* waves (e.g., Van Schaack et al., 1995), the orbital source generates *Sh* waves with large amplitudes for a wide range of vertical (borehole-parallel) source-receiver offsets. Also, OVS tends to generate only small tube waves (borehole-guided waves that are primarily supported by the compressional motion of the borehole fluid) that contaminate body waves used for seismic imaging (e.g., Cole, 1997). Furthermore, the source allows efficient decomposition of *Sh* and the other wave components through the superposition of phase-delayed, circularly polarized wave motions in both clockwise and counter-clockwise directions around the borehole (Daley and Cox, 2001).

Although many successful applications of the borehole orbital vibrator source have been reported during the past decade (Liu et al., 1991, 2000; Hardage, 1992), the mechanism of wave generation and the characteristics of waves generated by the orbital vibrator are not fully understood. A good, quantitative model is still needed that can predict the source characteristics such as the radiation pattern and tube wave generation, for applications such as anisotropy measurements and waveguide characterization of surrounding formations. Among several attempts to model the orbital vibrator source in the past, Dong (1994, 1995) developed a model based on the boundary element method. In this approach, the rotary motion of the vibrator was

incorporated into the form of a Green function for point sources that are distributed as a circular array around the borehole axis within the fluid. The model successfully predicted the generation of *Sh* waves as well as both *P* and *Sv* waves in both isotropic and anisotropic rocks around the borehole. However, the functional form of normal and shear forces applied to the borehole wall in this model was assumed rather than derived from actual vibrator motions, and only limited analysis was conducted using this model to examine the waves generated by an OVS.

In this paper, we introduce analytical models to examine the waves generated by an OVS. A two-dimensional model is first introduced that takes into account the mechanical interaction between a rigid source body with specified physical parameters and the surrounding borehole fluid and rock. Subsequently, a three-dimensional source model is proposed, that is conceptually similar to the model used by Kurkjian and Chang (1986) to examine the waves generated by stationary (non-rotating) multi-pole sources. The initially unknown source amplitude is determined using the two-dimensional model. These models have an advantage over fully numerical models based on finite difference methods and boundary element methods, because they allow us to analytically examine the relationship between OVS motions and borehole guided waves including tube waves. Using the introduced model, we will examine the radiation pattern of body waves generated by the orbital vibrator source and the characteristics of co-generated borehole-guided waves.

MODELING METHODS

2D representation of OVS

To determine the relationship between the wavefield generated by an OVS and physical source parameters, we first examine a two-dimensional model, assuming an infinitely long circular rigid source along the borehole, with a radius r_0 and a mass per unit length M_s (including an eccentric mass M_e, at a radius r_e), within a fluid-filled circular borehole with a radius a. Also, the rock surrounding the borehole is assumed to be isotropic and homogeneous. Although such generalization can be easily made, we do not assume a casing wall or mud-cake layers on the fluid-rock interface.

An OVS is driven by a centrifugal force $\mathbf{F}_e$ resulting from a spinning eccentric mass within the source, which is counteracted by the sum of fluid pressure $\mathbf{F}_p$ and the inertial force of the source. For stationary source motions with a circular frequency ω, this force equilibrium is written as

$$\mathbf{F}_e + \mathbf{F}_p = -(M_s - M_e)\omega^2 \mathbf{U}\,, \tag{1}$$

where **U** is the rigid body displacement of the source. In the following derivations, we assume that the magnitude of the centrifugal force is always given by $M_e r_e' \omega^2$ where $r_e' = r_e \cdot (M_s - M_e)/M_s$ is the radius of rotation around the center of the mass. Since the rotation results in a $\pi/2$ phase shift between the two orthogonal components of the force and displacement, using complex notations and Cartesian coordinates, the first term in Equation(1) can be computed by

$$\mathbf{F}_e = \begin{bmatrix} F_{ex} \\ F_{ey} \end{bmatrix} = M_e r_e' \omega^2 \begin{bmatrix} 1 \\ i \end{bmatrix} e^{-i\omega t}\,. \tag{2}$$

The source displacement is given by

$$\mathbf{U} = \begin{bmatrix} U_x \\ U_y \end{bmatrix} = U_0 \begin{bmatrix} 1 \\ i \end{bmatrix} e^{-i\omega t}\,. \tag{3}$$

It is the amplitude and phase of U_0 that we need to determine. This is done by applying a set of boundary conditions on the source-fluid boundary and the fluid-rock boundary.

To obtain an explicit form of solutions for the wavefield around the source, we assume that the particle motions induced by the source are small (less than 1 millimeter), and the source frequency is sufficiently low (below megahertz). As shown in Appendix A, under these assumptions, dthe isplacement and stress field around the source is acoustic, and the wavefield can be expressed by a superposition of cylindrical waves (Appendix B). The assumption for small amplitudes can be validated a posteori by using the source displacement amplitude obtained in this section using the acoustic approximation.

First, since the radial component of the source displacement U_r and the fluid displacement u_r have to be continuous on the source-fluid boundary at $r=r_0$,

$$u_r(r=r_0) = U_0(\cos\phi + i\sin\phi)e^{-i\omega t} = U_0 e^{i(\phi-\omega t)}$$
$$= \sum_{n=-\infty}^{\infty}\left[A_n^{P+}\partial_r H_n^{(1)}(k_{P1}r_0) + A_n^{P-}\partial_r H_n^{(2)}(k_{P1}r_0)\right]e^{i(n\phi-\omega t)}$$
$$\therefore U_0 = A_1^{P+}\partial_r H_1^{(1)}(k_{P1}r_0) + A_1^{P-}\partial_r H_1^{(2)}(k_{P1}r_0), \quad (4)$$

where ∂_r indicates partial derivative of the function via the radial variable *r*. Definitions for the unknown expansion coefficients are given in Appendex B. It is noted that this boundary condition leads to a requirement that all the terms $n \neq 1$ be identically zero. This forces both displacement and pressure field around OVS to be given by the first-order Bessel functions in the radial direction and by the first harmonic component in the angular direction. The latter characteristics indicates that OVS can be viewed as a rotating dipole source that generates rotating distribution of positive and negative pressure within the fluid, on the opposite sides of the circular body (Figure 2)

Next, the total force from the fluid pressure *p* surrounding the source is computed by

$$\mathbf{F}_p = \int_0^{2\pi}(-p)\begin{bmatrix}\cos\phi\\ \sin\phi\end{bmatrix}r_0 d\phi = -\rho_1\omega^2\int_0^{2\pi}\Phi_P^{(s)}\begin{bmatrix}\cos\phi\\ \sin\phi\end{bmatrix}r_0 d\phi$$
$$= -\rho_1\omega^2\left[A_1^{P+}(\omega)H_1^{(1)}(k_{P1}r_0) + A_1^{P-}(\omega)H_1^{(2)}(k_{P1}r_0)\right]\int_0^{2\pi}e^{i(\phi-\omega t)}\begin{bmatrix}\cos\phi\\ \sin\phi\end{bmatrix}r_0 d\phi, \quad (5)$$
$$= -\pi r_0\rho_1\omega^2\left[A_1^{P+}(\omega)H_1^{(1)}(k_{P1}r_0) + A_1^{P-}(\omega)H_1^{(2)}(k_{P1}r_0)\right]\begin{bmatrix}1\\ i\end{bmatrix}e^{-i\omega t}$$

where the relationship

$$-p = \rho_1 c_{P1}^2\nabla^2\Phi_P^{(s)} = -\rho_1\omega^2\Phi_P^{(s)} \quad (6)$$

was used for the 2D P-wave Helmholtz potential $\Phi_P^{(s)}$ for the source. From the force equilibrium in equation (1), using equations (2) and (5),

$$M_e r_e - \pi r_0\rho_1\left[A_1^{P+}H_1^{(1)}(k_{P1}r_0) + A_1^{P-}H_1^{(2)}(k_{P1}r_0)\right] = -(M_s - M_e)U_0, \quad (7)$$

where the common term $\omega^2\begin{bmatrix}1 & i\end{bmatrix}^T e^{-i\omega t}$ has been suppressed ("*T*" indicates the vector or matrix transposition). On the fluid-rock boundary at *r*=*a*, the radial component of both displacement and stress (pressure), u_r and σ_{rr}, respectively, is continuous, and the tangential (shear) component of stress, $\sigma_{r\phi}$, vanishes. These conditions respectively are

$$
\begin{aligned}
&u_r(r=a)\\
&=\partial_r H_1^{(1)}(k_{P1}a)A_1^{P+}+\partial_r H_1^{(2)}(k_{P1}a)A_1^{P-}=\partial_r H_1^{(1)}(k_{P2}a)B_1^{P}+(i/a)H_1^{(1)}(k_{S2}a)B_1^{S},
\end{aligned}
\tag{8}
$$

$$
\begin{aligned}
&\sigma_{rr}(r=a)\\
&=-\rho_1\omega^2\left[H_1^{(1)}(k_{P1}a)A_1^{P+}+H_1^{(2)}(k_{P1}a)A_1^{P-}\right]\\
&=\rho_2 c_{S2}^2\left[-\left(2D_r+k_{S2}^2\right)B_1^{P}H_1^{(1)}(k_{P2}a)+2iD_rB_1^{Sh}H_1^{(1)}(k_{S2}a)\right]
\end{aligned}
,
\tag{9}
$$

$$
\begin{aligned}
&\sigma_{r\phi}(r=a)=0\\
&=\rho_2 c_{S2}^2\left[2iD_rB_1^{P}H_1^{(1)}(k_{P2}a)+\left(2D_r+k_{S2}^2\right)B_1^{Sh}H_1^{(1)}(k_{S2}a)\right],
\end{aligned}
\tag{10}
$$

where we have introduced an operator

$$
D_r\equiv\frac{1}{r}\frac{\partial}{\partial r}-\frac{1}{r^2}=\frac{\partial}{\partial r}\frac{1}{r}.
\tag{11}
$$

The dependence on $e^{i(\phi-\omega t)}$ of all the terms in the above equations is understood and omitted. The above five boundary conditions are combined to obtain a linear system of equations

$$
\begin{bmatrix}
-\frac{M_s-M_e}{\pi r_0\rho_1} & H_1^{(1)}(k_{P1}r_0) & H_1^{(2)}(k_{P1}r_0) & 0 & 0\\
-1 & \partial_r H_1^{(1)}(k_{P1}r_0) & \partial_r H_1^{(2)}(k_{P1}r_0) & 0 & 0\\
0 & -\partial_r H_1^{(1)}(k_{P1}a) & -\partial_r H_1^{(2)}(k_{P1}a) & \partial_r H_1^{(1)}(k_{P2}a) & (i/a)H_1^{(1)}(k_{S2}a)\\
0 & -\rho_1\omega^2 H_1^{(1)}(k_{P1}a) & -\rho_1\omega^2 H_1^{(2)}(k_{P1}a) & \rho_2 c_{S2}^2\left(2D_r+k_{S2}^2\right)H_1^{(1)}(k_{P2}a) & -2i\rho_2 c_{S2}^2 D_r H_1^{(1)}(k_{S2}a)\\
0 & 0 & 0 & 2iD_rH_1^{(1)}(k_{P2}a) & \left(2D_r+k_{S2}^2\right)H_1^{(1)}(k_{S2}a)
\end{bmatrix}
\begin{bmatrix}
U_0\\ A_1^{P+}\\ A_1^{P-}\\ B_1^{P}\\ B_1^{Sh}
\end{bmatrix}
=
\begin{bmatrix}
\frac{M_e}{\pi r_0\rho_1}r_e\\ 0\\ 0\\ 0\\ 0
\end{bmatrix}.
\tag{12}
$$

The above matrix equation can easily be solved analytically. The solution for U_0 can be expressed as

$$
U_0=\left(-\frac{M_e}{M_s}r_e\right)\times\frac{1}{1-\frac{\pi r_0\rho_1}{M_s-M_e}\frac{d_1}{d_2}},
\tag{13}
$$

where

$$\begin{bmatrix} d_1 \\ d_2 \end{bmatrix} \equiv \mathbf{H}_{r_0} \left(\mathbf{H}_a \right)^{-1} \begin{bmatrix} c_1 \\ c_2 \end{bmatrix}, \tag{14}$$

$$\mathbf{H}_a \equiv \begin{bmatrix} H_1^{(1)}(k_{P1}a) & H_1^{(2)}(k_{P1}a) \\ \partial_r H_1^{(1)}(k_{P1}a) & \partial_r H_1^{(2)}(k_{P1}a) \end{bmatrix}, \tag{15}$$

$$\mathbf{H}_{r_0} \equiv \begin{bmatrix} H_1^{(1)}(k_{P1}r_0) & H_1^{(2)}(k_{P1}r_0) \\ \partial_r H_1^{(1)}(k_{P1}r_0) & \partial_r H_1^{(2)}(k_{P1}r_0) \end{bmatrix}, \tag{16}.$$

$$\begin{bmatrix} c_1 \\ c_2 \end{bmatrix} \equiv \begin{bmatrix} \frac{\rho_2}{\rho_1 k_{S2}^2}\left(2D_r + k_{S2}^2\right) H_1^{(1)}(k_{P2}a) & -\frac{\rho_2}{\rho_1 k_{S2}^2} \cdot 2iD_r H_1^{(1)}(k_{S2}a) \\ \partial_r H_1^{(1)}(k_{P2}a) & \frac{i}{a} H_1^{(1)}(k_{S2}a) \end{bmatrix} \begin{bmatrix} \left(2D_r + k_{S2}^2\right) H_1^{(1)}(k_{S2}a) \\ -2iD_r H_1^{(1)}(k_{P2}a) \end{bmatrix}. \tag{17}$$

The term in the parenthesis in equation (13) is the displacement of an OVS in the vacuum (or air), which is modified by the following term containing rock and borehole fluid properties.

For the special case of an OVS within an infinite fluid, the coefficients for waves propagating towards the source, A_1^{P-}, and the waves within the rock, B_1^P and B_1^{Sh}, can be set to zero. Therefore, equation (12) reduces to

$$\begin{bmatrix} -\frac{M_s - M_e}{\pi r_0 \rho_1} & H_1^{(1)}(k_{P1}r_0) \\ -1 & \partial_r H_1^{(1)}(k_{P1}r_0) \end{bmatrix} \begin{bmatrix} U_0^{\infty} \\ A_1^{P+} \end{bmatrix} = \begin{bmatrix} \frac{M_e}{\pi r_0 \rho_1} r_e' \\ 0 \end{bmatrix}, \tag{18}$$

which results in

$$U_0^{\infty} = \left(-\frac{M_e}{M_s} r_e \right) \times \frac{1}{1 - \frac{\pi r_0 \rho_1}{M_s - M_e} \frac{H_1^{(1)}(k_{P1}r_0)}{\partial_r H_1^{(1)}(k_{P1}r_0)}}, \tag{19}$$

and the source potential

$$\Phi_P^{(s)} = A_1^{P+} H_1^{(1)}(k_{P1}r) e^{i(\phi - \omega t)} = \frac{U_0^{\infty}}{\partial_r H_1^{(1)}(k_{P1}r_0)} H_1^{(1)}(k_{P1}r) e^{i(\phi - \omega t)}. \tag{20}$$

This result is used to determine the amplitude of a three-dimensional OVS in the next section.

In Figure 3, the source displacement amplitude is shown as a function of frequency, for sources within vacuum, infinite fluid, and borehole fluid surrounded by rock. The model parameters used in this example are shown in Table 1. It can be seen that the displacement amplitudes of the source for the frequencies of our interest (70 Hz~400 Hz) are nearly constant.

Also, the amplitude of the sources within an infinite fluid and a finite-diameter borehole are reduced from a source within a vacuum due to the impedance effect of the surroundings.

Table 1 Model parameters

Baseline material parameters			Source/borehole parameters		
Flud density	ρ_1	1000 g/cm^3	Source length	L	61.0 cm
Fluid P velocity	c_{P1}	1460 m/s	Source radius	r_0	5.08 cm
Rock density	ρ_2	2100 g/cm^3	Source mass per length	M_s	14.9 kg/m
Rock P velocity	c_{P2}	3000 m/s	Eccentric mass radius	r_e	7.29 mm
Rock S velocity	c_{S2}	1731 m/s	Eccentric mass per length	M_e	1.62 kg/m
			Borehole diameter	a	7.62 cm

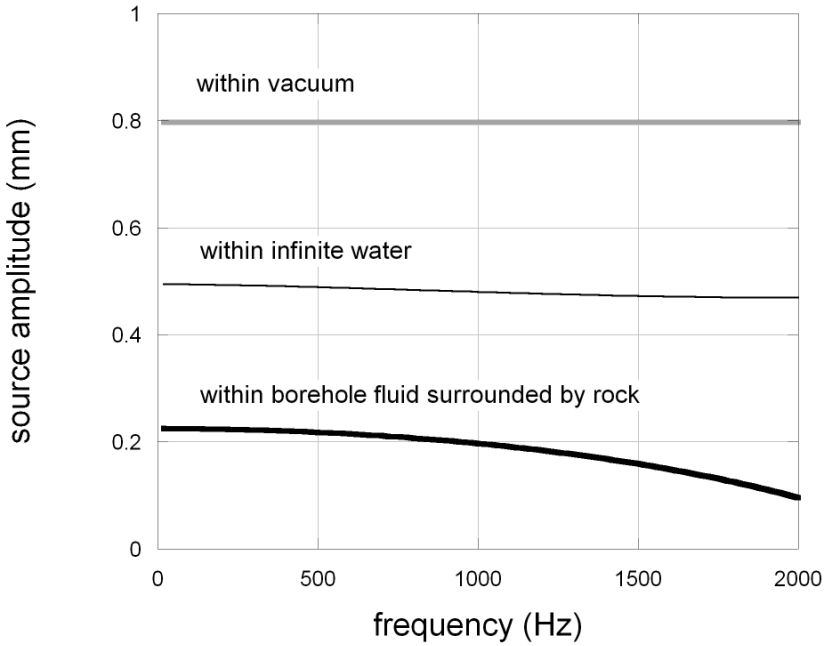

FIG. 3. A comparison of source displacements for OVS's suspended in the vacuum (air), infinite water, and a fluid-filled borehole within rock. The baseline source and material parameters are given in Table 1.

3D representation of OVS

Unlike the two-dimensional case, three-dimensional geometry of an OVS is difficult to model analytically. As an alternative, we represent the source by a circular array of phase-delayed point dilatation (or volume displacement) sources located around the borehole axis. This representation of a borehole source is similar to the Kurkjian and Chang (1986)'s model used to examine the waves generated by fluid-coupled, multi-pole borehole sources for well logging.

Phase delays between the individual sources of the Kurkjian and Chang's model are either 0 or π radians. In contrast, phase delays within the point source array for the orbital vibrator source change continuously from 0 to 2π (counter-clockwise spin) or 0 to -2π (clockwise spin).

Using the partial wave expansion technique, the radiation and scattering of the waves generated by OVS can be examined analytically using the frequency-wavenumber integration techinique and solved numerically by the discrete wavenumber method. A single time-harmonic volume source with a magnitude $V_0(\omega)$, located at the center of infinite acoustic medium, generates a wavefield with a single scalar Helmholtz potential given by (e.g., Lee and Balch, 1982; Kurkjian and Chang, 1986)

$$-\frac{V_0(\omega)}{4\pi R}\mathrm{e}^{i\omega(R/c_{P1}-t)} = -\frac{iV_0(\omega)}{8\pi}\int_{-\infty}^{+\infty} H_0^{(1)}(k_r^{P1}r')\,\mathrm{e}^{i(k_z z-\omega t)}\,dk_z\,, \tag{21}$$

where R is the source-receiver distance, $k_r^{P1}=\sqrt{(\omega/c_{P1})^2-k_z^2}$ where k_z is the z-direction (borehole-parallel) wavenumber, and r' is the projection of R onto the plane perpendicular to the z or borehole axis. In the above expression, V_0 has a dimension of [Volume/Length] for a single circular array of point sources (1D array), and [Volume/Length^2] for circular arrays distributed also in the z direction (2D array). Throughout the rest of this article, the positive and negative sign conventions are used for wavenumbers and frequencies, respectively, as in equation (21). Also, since wavenumber components are examined individually, the above source potential term is

$$s_{V_0} = -\frac{iV_0(\omega)}{8\pi}H_0^{(1)}(k_r^{P1}r')e^{i(k_z z-\omega t)}\,. \tag{22}$$

We represent an OVS, located on the borehole axis and with a vibration frequency ω, as a series of point volume sources located at a radius r=r_0 around the borehole axis (Figure 4). Each source, located at an angular coordinate θ measured from the x axis, has a phase delay exp($i\theta$), resulting in a constant phase rotating around the borehole axis at a spin frequency ω.

To compute the superimposed effect of the off-centered point sources, we first examine the waves generated by a single point source at (r_0, θ). The origin of the coordinate in equation (22) is shifted along the x' axis by r_0 (Figure 4b). This involves a coordinate transform via

$$r\cos(\phi-\theta) = r_0 + r'\cos\psi\,, \tag{23}$$

$$r\sin(\phi-\theta) = r'\sin\psi\,, \tag{24}$$

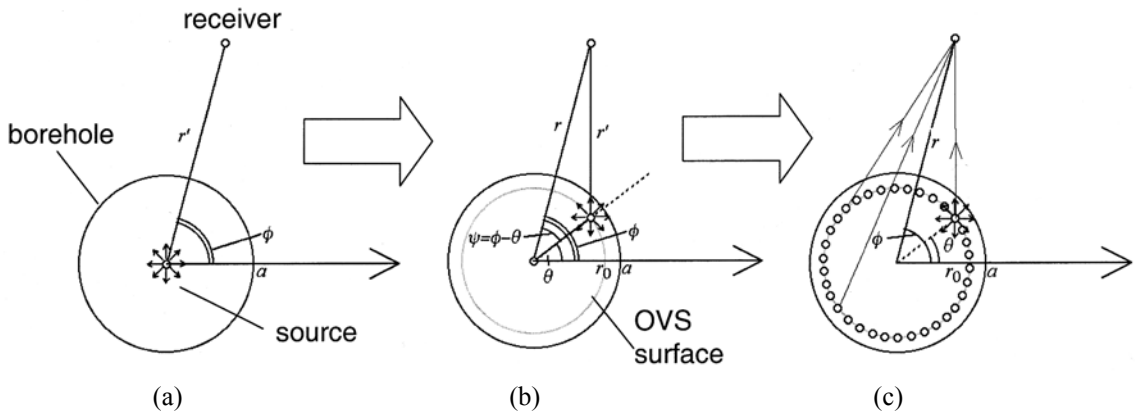

FIG. 4. Representation of a 3D OVS using point volumetric sources. A single point volume source (left) is first shifted to the radius of the OVS. Subsequently, the source potentials for these shifted point sources (center) are superposed with a phase shift that continuously changes around the OVS.

where r and ϕ are the radial and angular coordinates of the receiver, ψ is the angular coordinate of the receiver measured from the x' axis. Equations (23) and (24) implies

$$r' = \sqrt{r^2 + r_0^2 - 2rr_0\cos(\phi - \theta)}\ . \tag{25}$$

Using equation (25), the potential given by a single Hankel function around the source is expressed via an infinite series of partial waves using the relationships

$$\begin{aligned} &H_0^{(1)}(k_r^{P1}r') = H_0^{(1)}(k_r^{P1}\sqrt{r^2 + r_0^2 - 2rr_0\cos(\phi-\theta)}) \\ &= \sum_{n=-\infty}^{\infty} \begin{Bmatrix} J_n(k_r^{P1}r_0)H_n^{(1)}(k_r^{P1}r)\ (\text{if } r > r_0 \geq 0) \\ J_n(k_r^{P1}r)H_n^{(1)}(k_r^{P1}r_0)\ (\text{if } r_0 > r \geq 0) \end{Bmatrix} \cdot \exp in(\phi - \theta) \end{aligned}\ . \tag{26}$$

The overall effect of the phase-delayed sources (Figure 4c) is computed by introducing the equation (26) into equation (22) and integrating the resulting expression with a phase delay factor $\exp i\theta$ over the values of the angle $0<\theta<2\pi$. For reasons that will become clear shortly, we will generalize this delay factor as $\exp(im\theta)$ (m=…-2, -1, 0, 1, 2,…). OVS's with these delay factors can be viewed as "generalized" OVS's with multiple cycles of pressure oscillation around the source. The angular integration with these delay factors involves the orthogonality relationship

$$\int_0^{2\pi} e^{in(\phi-\theta)} \cdot e^{im\theta} d\theta = 2\pi \cdot e^{in\phi}\delta_{m,n}\ , \tag{27}$$

where $\delta_{m,n}$ is the Kronecker delta. Using the relationship (27), the source potential for a 1D array is given by

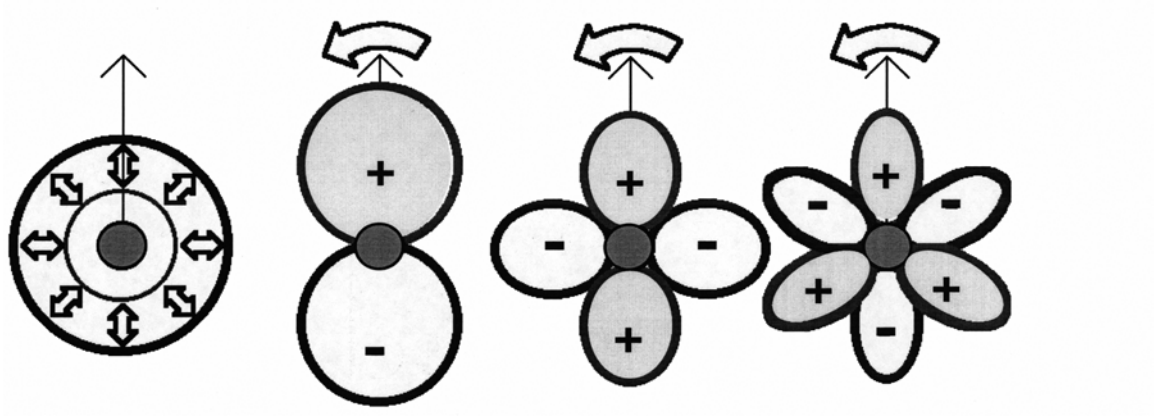

m=0 m=1 m=2 m=3

FIG. 5 Distribution of fluid pressure perturbation around OVS's with different orders. Except for the 0 th order source (monopole), these sources can be viewed as rotating multi-pole sources (order m).

$$\Phi_P^{(s)}(z) = \int_0^{2\pi} s_{V_0} e^{im\theta} r_0 d\theta$$

$$= -\frac{iV_0(\omega)}{8\pi} r_0 e^{i(k_z z-\omega t)} \sum_{n=-\infty}^{\infty} \begin{Bmatrix} J_n(k_r^{P1} r_0) H_n^{(1)}(k_r^{P1} r) \text{ (if } r > r_0 \geq 0) \\ J_n(k_r^{P1} r) H_n^{(1)}(k_r^{P1} r_0) \text{ (if } r_0 > r \geq 0) \end{Bmatrix} \cdot \int_0^{2\pi} e^{in(\phi-\theta)} \cdot e^{im\theta} d\theta$$

$$= -\frac{iV_0(\omega)}{4} r_0 \begin{Bmatrix} J_m(k_r^{P1} r_0) H_m^{(1)}(k_r^{P1} r) \text{ (if } r > r_0 \geq 0) \\ J_m(k_r^{P1} r) H_m^{(1)}(k_r^{P1} r_0) \text{ (if } r_0 > r \geq 0) \end{Bmatrix} \cdot e^{i(m\phi + k_z z-\omega t)}. \quad (28)$$

An OVS with a finite length (i..e., 2D array) can be modeled by the superposition of the above sources distributed along the borehole axis. For vibrator length L, equation (28) is integrated for sources distributed along the borehole axis, resulting in

$$\Phi_P^{(s)}(z;L) = \int_{-L/2}^{+L/2} \Phi_P^{(1)}(z-\zeta) d\zeta$$

$$= \Phi_P^{(s)}(z) \int_{-L/2}^{+L/2} \exp(-ik_z\zeta) d\zeta = \Phi_P^{(s)}(z) \cdot L \cdot \frac{\sin(k_z L/2)}{k_z L/2}, \quad (29)$$

which is the source potential for the 1D array modulated by a sinc (sampling) function. Note that the dimension of the source potential is different between the single array and the distributed array (finite length source).

The above results indicate that the phase delay among the point sources constituting an OVS selects a single term out of the infinite series of the partial wave expansion. From equation (28), a ring-shaped expansion source (e.g., Dong et al., 1995) can be viewed as a generalized orbital

source of the order m =0, and the currently used mechanical OVS as the order m=1. Pressure distribution around the generalized OVS's is shown schematically in Figure 5. These sources can be viewed as the multipole sources used for S-wave borehole logging (Chen and Eriksen, 1991) that rotate around the borehole axis. It is also noted that the superposition of the two sources of the same order but with opposite spin directions results in

$$\begin{aligned}&\Phi_P^{(s)}(m)+\Phi_P^{(s)}(-m)\\&=-\frac{iV_0(\omega)}{2}r_0\sigma\begin{Bmatrix}J_m(k_r^{P1}r_0)H_m^{(1)}(k_r^{P1}r)\ (\text{if } r>r_0\ge 0)\\J_m(k_r^{P1}r)H_m^{(1)}(k_r^{P1}r_0)\ (\text{if } r_0>r\ge 0)\end{Bmatrix}\cdot\cos(m\phi)\cdot e^{i(k_z z-\omega t)},\end{aligned}\qquad(30)$$

which is the stationary (non-rotating) multi-pole source solution examined by Kurkjian and Chang (1986).

For the m=1 source, it is possible to relate self-consistently the point volume source amplitude $V_0(\omega)$ to the physical source parameters as we did for the 2D OVS. It is noted, however, that the source amplitude is not only a function of source parameters but also is dependent upon the borehole geometry and material properties of the surrounding fluid and rock. As an approximation, we derive an expression of $V_0(\omega)$ for the OVS in an infinite fluid as a function of source parameters and fluid properties. This is done by making the length of the source infinitely long, and also integrating for all the wavenumbers:

$$\begin{aligned}\Phi_{P,2D}^{(s)}&=\int_{-\infty}^{+\infty}\lim_{L\to\infty}\Phi_P^{(1)}(z;L)dk_z=\int_{-\infty}^{+\infty}\Phi_P^{(s)}(z)\cdot\lim_{L\to\infty}\frac{\sin(k_zL/2)}{k_z/2}dk_z\\&=\int_{-\infty}^{+\infty}\Phi_P^{(s)}(z)\cdot 2\pi\delta(k_z)dk_z=-V_0(\omega)\frac{i\pi r_0}{2}J_1(k_{P1}r_0)H_1^{(1)}(k_{P1}r)\,\mathrm{e}^{i(\phi-\omega t)}\end{aligned},\qquad(31)$$

where $\delta(k_z)$ is the Dirac delta function. By comparing equation (31) to equation (20),

$$V_0(\omega)=\frac{2iU_0^{\infty}}{\pi r_0 J_1(k_{P1}r_0)\partial_r H_1^{(1)}(k_{P1}r_0)},\qquad(32)$$

where U_0^{∞} is the complex source amplitude in equation (19) containing physical source parameters.

For three-dimensional problems, the boundary conditions used to solve for the unknown coefficients A_n^P, B_n^P, B_n^{Sh}, and B_n^{Sv} in the series expansions of displacement in Appendix B are the continuity of radial displacement and normal stress (pressure), and two vanishing shear stress components on the borehole wall. These four conditions can be applied to obtain a linear system

of equations for the four coefficients for individual modes n. Note that an OVS of the order m can excite only the n=m th partial waves. The resulting linear system of equations is

$$\times\begin{bmatrix} J_m(k_r^{P1}a) & & & \\ & H_m^{(1)}(k_r^{P2}a) & & \\ & & H_m^{(1)}(k_r^{S2}a) & \\ & & & H_m^{(1)}(k_r^{S2}a) \end{bmatrix}\begin{Bmatrix} A_m^P \\ B_m^P \\ B_m^{Sh} \\ B_m^{Sv} \end{Bmatrix} \equiv \mathbf{M}_m \begin{Bmatrix} A_m^P \\ B_m^P \\ B_m^{Sh} \\ B_m^{Sv} \end{Bmatrix} = \mathbf{s}_m , \tag{33}$$

where $\mathbf{s}_m$ is the source term computed from equation (28)

$$\begin{bmatrix} -\partial_{P1} & \partial_{P2} & im & ik_z a\partial_{S2} \\ (1/\mu_2)\rho_1\omega^2 a^2 & -(\lambda_2/\mu_2)k_{P2}^2 a^2 + 2\partial_{P2}^2 & 2im(-1+\partial_{S2}) & 2ik_z a\partial_{S2}^2 \\ 0 & im(-2+\partial_{P2}) + im\partial_{P2} & -\partial_{S2}^2 + \partial_{S2} - m^2 & -2mk_z a(-1+\partial_{S2}) \\ 0 & 2ik_z a\partial_{P2} & -mk_z a & ((k_r^{S2}a)^2 - (k_z a)^2)\partial_{S2} \end{bmatrix}$$

$$\mathbf{s}_m = -\frac{iV_0(\omega)}{4} r_0 J_m(k_r^{P1} r_0) \begin{Bmatrix} \partial_{P1} \\ -\rho_1 a^2\omega^2/\mu_2 \\ 0 \\ 0 \end{Bmatrix} H_m^{(1)}(k_r^{P1}a) . \tag{34}$$

Equations (21) and (22) can be derived from the source potentials in equations (8) and (12). In the above equations, the symbols ∂_P and ∂_S, with numbers in the subscripts denoting either 1=inside or 2=outside the borehole, are defined as

$$\partial_{P,S} Z_m \equiv (k_r^{P,S}a)\left.\frac{dZ_m(z)}{dz}\right|_{z=k_r^{P,S}a}, \tag{35}$$

where Z_m are Bessel functions of appropriate kind. Also it is noted that equations (21), (22), and (23) are scaled by the borehole radius a. These equations can be constructed and solved for a given combination of a wave frequency and a z-direction wavenumber. The displacements are computed by introducing the resulting potentials into equations (B2), (B3), and (B4).

EXAMPLES AND DISCUSSIONS

Comparison of 2D physical and fictitious OVS

We derived the three-dimensional OVS model by imposing a radial out-going wavefield within the borehole fluid (a "fictitious" source). This approach, however, does not take into

account the interaction of the source and the waves reflected by the borehole wall. To estimate the error introduced by this approximation, we compare the waves generated by a physical source in the section "2D representation of OVS", and the waves generated by the fictitious source which are computed by embedding the two-dimensional out-going wavefield from OVS within an infinite fluid.

For the fictitious source, the wavefiled within the borehole is given by a superposition of the source wavefield and the acoustic wavefiled that is non-singular at the center of the borehole, which forces the use of the Bessel function of the 1st kind. The system equation to be solved is

$$\begin{bmatrix} -\partial_r J_1(k_{P1}a) & \partial_r H_1^{(1)}(k_{P2}a) & (i/a)H_1^{(1)}(k_{S2}a) \\ -\rho_1\omega^2 J_1(k_{P1}a) & \rho_2 c_{S2}^2\left(2D_r + k_{S2}^2\right)H_1^{(1)}(k_{P2}a) & -2i\rho_2 c_{S2}^2 D_r H_1^{(1)}(k_{S2}a) \\ 0 & 2iD_r H_1^{(1)}(k_{P2}a) & \left(2D_r + k_{S2}^2\right)H_1^{(1)}(k_{S2}a) \end{bmatrix} \begin{bmatrix} A_1^P \\ B_1^P \\ B_1^{Sh} \end{bmatrix} = \begin{bmatrix} \partial_r H_1^{(1)}(k_{P1}a) \\ \rho_1\omega^2 H_1^{(1)}(k_{P1}a) \\ 0 \end{bmatrix} \times \frac{U_0^\infty}{\partial_r H_1^{(1)}(k_{P1}a)} \tag{36}$$

Comparing the solutions from equations (36) and (12), the accuracy of the approximation can be evaluated.

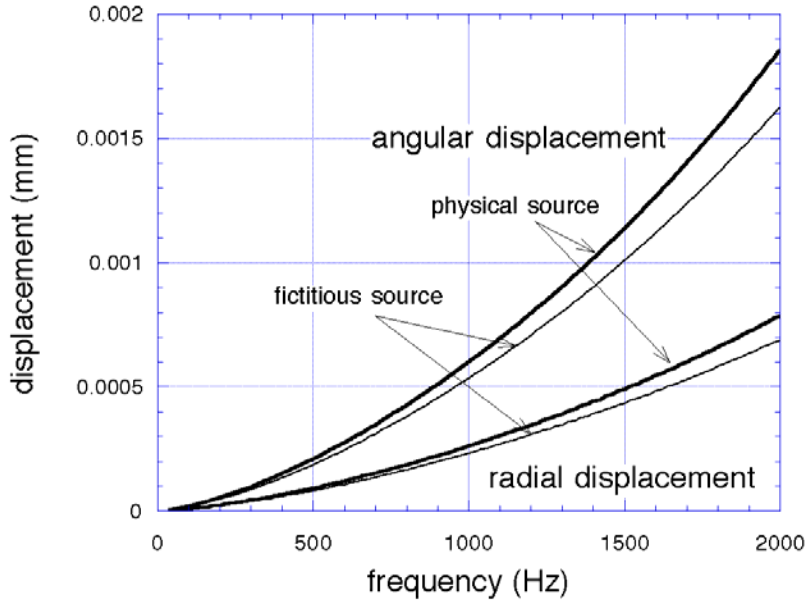

FIG. 6 A comparison of radial (primarily due to P waves) and angular (primarily due to S waves) displacements for the physical and fictitious sources measured 100 m away from the 2D OVS's. The fictitious sources somewhat underestimates the amplitudes of the generated waves.

Figure 6 shows a comparison of P and S wave amplitudes in the rock at a receiver located 100 m away from the source. The model parameters are the ones shown in Table 1. This example shows that the amplitude of the waves from using the fictitious source is 5 to 10% smaller than the physical source for up to several kilohertz.

The "driving-point impedance effect" of 2D OVS

As we saw in Figure 3, the amplitude of the source motion is dependent on the physical properties of surrounding rocks. This indicates that the source motion of an OVS tool itself can be used for borehole logging of rock properties. This idea has been introduced and both theoretically and experimentally examined by Novascone et al. (2002) who termed this the driving point impedance effect.

Using the two-dimensional OVS model in equation (13), we can perform a series of sensitivity studies for the rock properties (density, P and S wave velocities). Again, using the baseline properties in Table 1, the amplitudes of the source as a function of wave frequency and rock properties are shown in Figure 7. From Figure 7a it can be seen that the source motion is practically insensitive to the formation P wave velocity for the frequencies of our interest (below a few kilohertz). In contrast, the source motion shows appreciable sensitivity to the density and S wave velocity (Figure 7b and 7c). However, in general, the sensitivity is very small for frequencies below the current maximum operational frequency of 400 Hz. For very small S-wave formation velocities, however, the weak (attenuated) resonance of the system shifts to lower frequencies, causing significant changes in the source amplitude. In the zero S-wave velocity limit, the source amplitude approaches the amplitude of OVS within an infinite fluid.

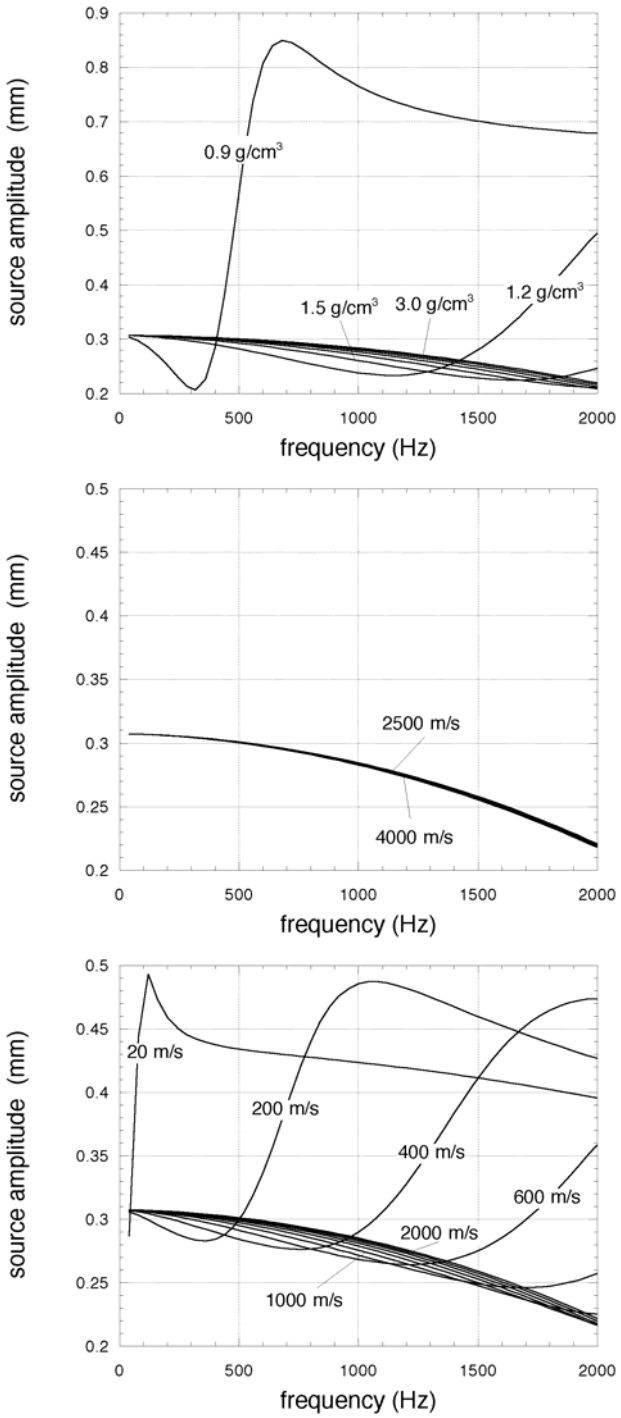

(a) Density sensitivity

(b) P-wave velocity sensitivity

(c) S-wave velocity sensitivity

FIG. 7 Parametric study of the 2D OVS displacement using the baseline properties shown in Table 1. For a practical range of material properties, OVS's show some sensitivity to the formation density and S wave velocity, but little sensitivity to the P wave velocity.

Radiation pattern of a 3D OVS

Using the discrete wavenumber method, the displacement wavefield generated by orbital vibrator sources of different orders can be computed to study the radiation characteristics of the source. The following examples are given for the parameters in Table 1, and a frequency of 200 Hz and a source-to-receiver distance of 100 m. The point volume source amplitude (V_0) of all the sources are given by equation (32), even for sources with the order $m \neq 1$. Also, for the stability of the wavenumber integration, we assumed small attenuation in the rock (seismic quality factor Q=500) and rather large attenuation in the fluid Q=100). The large quality factor was used in the fluid in order to suppress the tube waves, and this has very small effect on the radiation pattern of the bodywaves.

The order m=0 OVS is a ring-shaped explosion source (monopole), and the radiation patterns of the generated waves are very similar to those of a single point volume source located on the borehole axis. Amplitudes of the displacement in a single radial plane are shown in Figure 8a, as a function of the dip angle Θ from the source plane. Because of the angular symmetry of the source, *Sh* waves are not generated. From the figure it can be seen that this type of source generates *P* waves (shown as P(xz) in the figure) that have a radiation pattern with a wide angular coverage in the vertical directions. The source also generates *Sv* waves (shown as S(xz)) with significant amplitudes. However, the amplitude of the *Sv* waves diminishes to zero in the zero vertical offset directions, which is not desirable for cross-well measurements of waves. It is also noted that this type of source generates large tube waves as shown in the plot.

In contrast, the currently used OVS (m=1) generates significantly large *Sh* waves compared to *P* waves, respectively shown as S(θ) and P(xz) in Figure 8b. The overall magnitude of the waves, however, is much smaller than the m=0 th mode source, because dipole sources are not as effective as monopole sources. The radiation pattern of the *Sh* waves is nearly spherical, which is an ideal property as a borehole source for the seismic imaging of the surrounding rocks. Further, no significant amplitude of borehole-guided waves are seen near the borehole.

For higher order modes, the amplitudes of the waves generated by the vibrator become increasingly smaller. However, *Sh* waves are always generated by the sources, and their relative amplitudes compared to the P waves are significantly large. Radiation patterns for the modes

m>1 maintain a good coverage over a wide range of vertical offset angles except for the angles near borehole-parallel directions. An example for the m=2 nd mode is shown in Figure 8 (right).

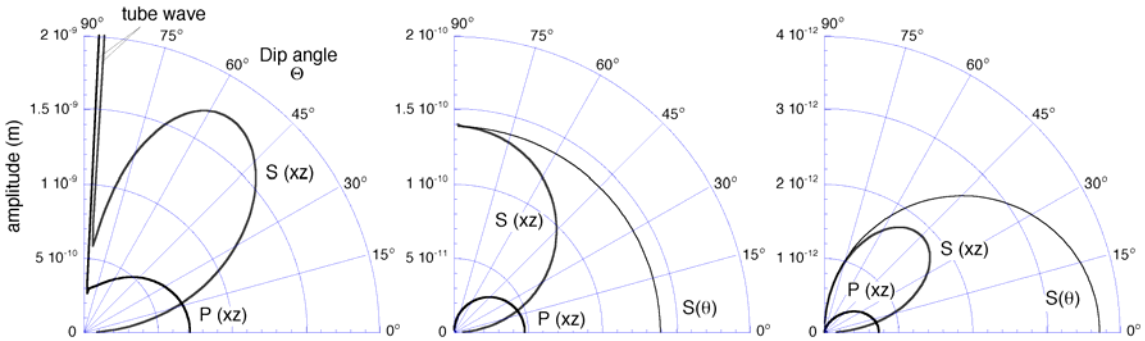

(a) m=0 (b) m=1 (c) m=2

FIG. 8 Radiation pattern of waves generated by OVS's of order m=0 (left, monopole), m=1 (center, dipole), and m=2 (right, quadrupole). "P(xz)" and "S(xz)" indicate displacement components of P and S waves within the plane parallel to the borehole, and "S(θ)" indicates the S wave amplitude normal to the borehole, respectively. P(xz) closely equals the P wave amplitude, and S(xz) and S(q) are the Sv and Sh wave amplitudes, respectively.

Borehole-guided waves

An orbital vibrator source generates guided waves along the borehole. For the m th order source, an infinite series of guided waves is generated, that is characterized by the dispersion equation

$$\det[\mathbf{M}_m(k_z,\omega)]=0, \qquad (37)$$

where $\mathbf{M}_m$ is the matrix given by equation (33). Similar to the body waves, an OVS of order m can generated only the guided waves of the order M=m. It is noted that these equations are the dispersion equations of borehole guided waves of arbitrary radial and circumferential orders. For the case m=0, equation (37) becomes the dispersion equation for the borehole guided waves studied by Biot (1952), which has an infinite number of solutions. For m=0, the fundamental mode of the solutions for this equation is known as a tube wave which, for borehole fluids with P-wave velocity lower than the surrounding rock's S-wave velocity, exists at all frequencies and propagates at velocities less than the P-wave velocity of the borehole fluid. For $m \geq 1$, equation (37) also generates an infinite number of solutions for each m. However, the fundamental mode of these solutions does not propagate (complex-valued solution) at low frequencies. As an

example, the phase velocity dispersion of the fundamental modes of order M=0, 1, 2, and 3 is shown in Figure 9 (for properties in Table 1).

A unique property of the orbital vibrator-generated borehole-guided waves with higher circumferential orders ($m \geq 1$) is that the mode shapes of the tube waves rotate around the borehole axis as the wave propagates along the borehole. Because of this, the mode shapes have a "twisted" appearance around the borehole axis (Figure 10). The dispersion characteristics of these guided waves, however, are the same as the guided waves generated by conventional sources (e.g., Paillet and White, 1982), because the dispersion equation (37) is irrelevant to the source term.

An important consequence of the mode-selective property of the orbital vibrator source is that, except for the m=0 case, body waves are generated below the cut-off frequency of the related guided waves. This should improve the quality of body wave seismograms measured using the orbital vibrator source by reducing the noise originated by borehole guided waves. However, this may not be the case when the polar symmetry in the geometry of the borehole and the vibrator body is broken due to the heterogeneity in the surrounding rocks, a wash-out zone around the borehole, and the shifted center of the vibrator axis off the borehole axis: an

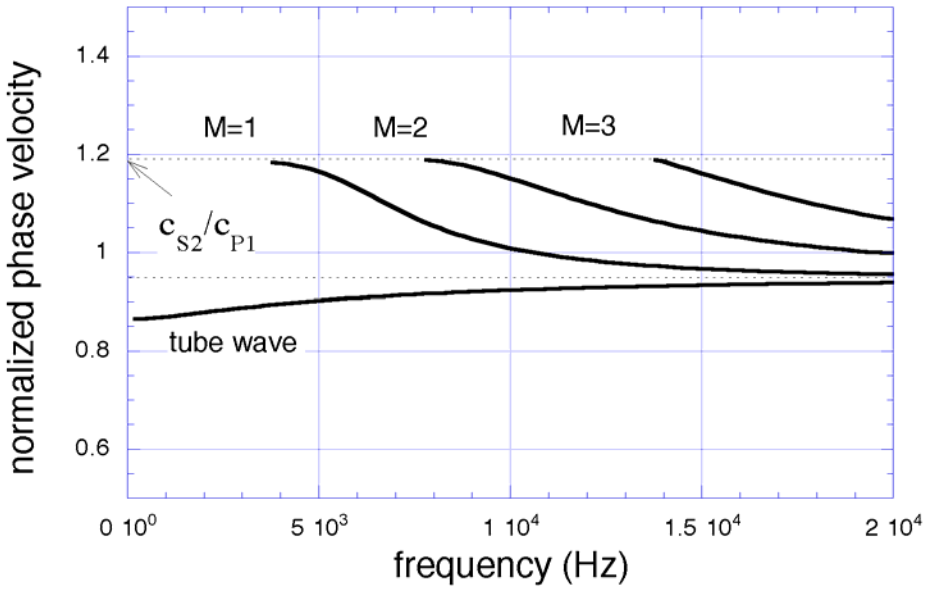

FIG. 9 Dispersion of fundamental mode borehole guided waves generated by order m=M OVS's. Velocities are normalized by the fluid P-wave velocity. M=0 corresponds to the tube waves. For higher-order sources (M>0), the guided waves have cut-off frequencies that are well above the frequencies used in the field.

imperfect mode selection results in the generation tube waves. Although the effect of misalignment can be examined analytically (e.g, Nakagawa & Daley, 2003), the effect of heterogeneity has to be examined using numerical simulations.

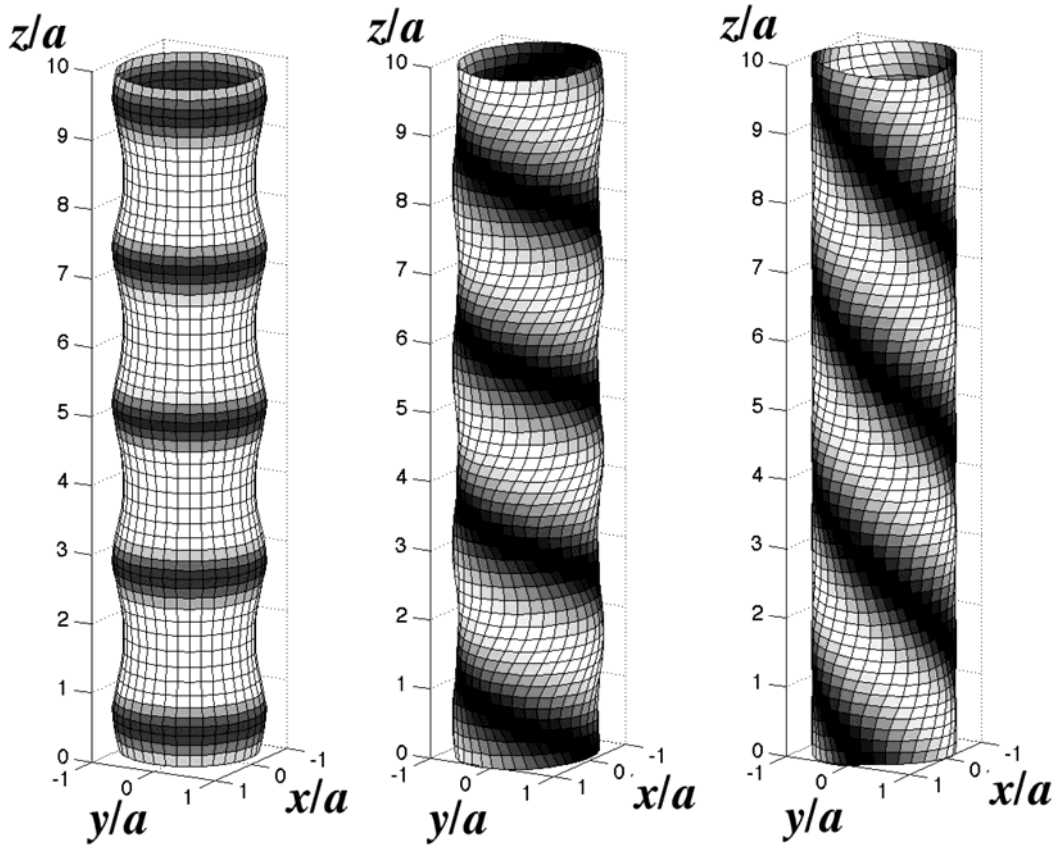

(a) M=0 (b) M=1 (c) M=2

FIG. 10 Borehole-wall mode shapes of borehole guided waves (fundamental modes) for generalized OVS of order m=0 (left), m=1 (center), and m=2 (right). To compare the mode shapes of propagating guided waves, a high, single frequency of 15 kHz was selected. Light and Dark colors indicate low and high fluid pressure on the wall. Due to the rotation of the source, the higher-order modes have a 'twisted' mode shape.

CONCLUSIONS

In this article we presented analytical models for the orbital vibrator source: A fluid-coupled, borehole shear wave source. A two-dimensional model was developed based upon physical source while a three-dimensional model was developed using single and distributed arrays of point sources.

From the model derivation, it can be seen that the fundamental mechanism of S wave generation by an OVS is the conversion of P waves into S waves on the borehole wall. However, since the source acts as a rotating dipole, the source is not as efficient as monopole sources. Although an OVS is a fluid-couple source, the 2D model indicates that the source motion itself is insensitive to P-wave acoustic impedance of the formation while somewhat dependent on the S-wave impedance. This can be explained by the dipole (or multi-pole) nature of the source, because the net volume change within the borehole fluid is zero: the same mechanism utilized by the dipole logging tools. The 2D source model is also useful for examining the relationship between the source parameters and the amplitudes of generated waves. However, the relationships may not be accurate quantitatively because the model assumes an infinite source length.

The 3D source predicts very uniform, spherical radiation pattern of *Sh* waves generated by OVS, which confirms field observations that the source can be used for wide-angle crosshole, VSP, and singlehole seismic measurements. Further, the theory indicates that, under ideal conditions, OVS should generate no borehole-guided waves at frequencies used in the field. This is not usually the case for real measurements where OVS is located off the borehole axis and heterogeneities are present in the formation surrounding the borehole. The effect of heterogeneity, and the background formation structures and anisotropy, is difficult to examine using the proposed semi-analytical model, and needs to be studied numerically. The model presented in this article, however, provides clear physical insights into the mechanism of wave generation, and a quick tool to estimate the amplitude and radiation of waves generated by OVS.

ACKNOWLEDGMENTS

This research has been supported by the Office of Science, Office of Basic Energy Sciences, Division of Chemical Sciences of the U.S. Department of Energy under contract No. DE-AC76SF00098. The author would like to thank Dr. Steven R. Pride (Lawrence Berkeley National Laboratory) for the discussion regarding the validity of the acoustic approximation used in the source modeling.

APPENDIX A Justification for the use of acoustic wave equation in borehole fluid

The Navier-Stokes equation for wave propagation within the borehole fluid is

$$\rho_f(\frac{\partial}{\partial t}\mathbf{v}+\mathbf{v}\cdot\nabla\mathbf{v})=\mu_f\nabla^2\mathbf{v}-\nabla p+(\mu_f/3+\lambda_f)\nabla\nabla\cdot\mathbf{v}, \tag{A1}$$

where ρ_f is the fluid density, and μ_f and λ_f are the shear and bulk viscosity. By taking the divergence and time derivation of the above equation, and also from the constitutive relationship

$$\nabla\cdot\mathbf{v}=-\frac{1}{K_f}\frac{\partial p}{\partial t}, \tag{A2}$$

we obtain

$$\begin{aligned}&\rho_f\frac{\partial^2}{\partial t^2}(\nabla\cdot\mathbf{v})+\rho_f\frac{\partial}{\partial t}\nabla\cdot(\mathbf{v}\cdot\nabla\mathbf{v})\\&=K_f\nabla^2(\nabla\cdot\mathbf{v})+(4\mu_f/3+\lambda_f)\frac{\partial}{\partial t}\nabla^2(\nabla\cdot\mathbf{v})\end{aligned}. \tag{A3}$$

K_f is the fluid bulk modulus. We first compare the two terms on the right hand side of the equation. By replacing the time derivative by -$i\omega t$, the relative magnitude of the second term with respect to the first term is

$$\frac{(4\mu_f/3+\lambda_f)\omega}{K_f}=\frac{4/3\cdot10^{-3}+2.8\cdot10^{-3}}{2.25\times10^{9}}\omega=(1.15\times10^{-11})\times f, \tag{A4}$$

Therefore, the viscosity term can be neglected for all frequencies of interest for our problems (up to several kilohertz).

Next, we evaluate the relative magnitude of the second term (nonlinear convection term) of the left hand side of the equation against the first term. Here, as an approximation, we replace the nabra operator ∇ by the inverse of a characteristic length, e.g., the source radius. By using the approximate source displacement, u=0.5 mm, from the two-dimensional analysis, this yields

$$\left|\frac{\rho_f\omega\nabla\cdot(\mathbf{v}\cdot\nabla\mathbf{v})}{\rho_f\omega^2(\nabla\cdot\mathbf{v})}\right|\approx\frac{u}{a}=\frac{0.5\times10^{-3}}{50\times10^{-3}}=0.01\ll 1. \tag{A5}$$

Therefore, the nonlinear term can be neglected.

Returning to the original equation without the nonlinear and viscosity terms, by applying the divergence to the equation and using the constitutive equation,

$$\frac{\rho_f}{K_f}\frac{\partial^2}{\partial t^2}p = \nabla^2 p\,. \tag{A6}$$

This is the acoustic wave equation.

APPENDIX B Partial wave expansion of solutions in cylindrical coordinates

The wavefield outside the borehole can be computed from three scalar displacement potentials Φ_P, Φ_{Sh}, and Φ_{Sv}. The components of displacement are computed using these potentials as (e.g., Kurkjian and Chang, 1986)

$$\mathbf{u} = \nabla\Phi_P + \nabla\times(\hat{\mathbf{z}}\Phi_{Sh}) + \nabla\times\nabla\times(\hat{\mathbf{z}}\Phi_{Sv}) . \tag{B1}$$

In cylindrical coordinates, the components of the displacement are

$$u_r = \frac{\partial\Phi_P}{\partial r} + \frac{1}{r}\frac{\partial\Phi_{Sh}}{\partial\phi} + \frac{\partial^2\Phi_{Sv}}{\partial r\partial z}, \tag{B2}$$

$$u_\phi = \frac{1}{r}\frac{\partial\Phi_P}{\partial\phi} - \frac{\partial\Phi_{Sh}}{\partial r} + \frac{1}{r}\frac{\partial^2\Phi_{Sv}}{\partial\phi\partial z}, \tag{B3}$$

$$u_z = \frac{\partial\Phi_P}{\partial z} - \frac{\partial^2\Phi_{Sv}}{\partial r^2} - \frac{1}{r}\frac{\partial\Phi_{Sv}}{\partial r} - \frac{1}{r^2}\frac{\partial^2\Phi_{Sv}}{\partial\phi^2} . \tag{B4}$$

For the acoustic fluid within a borehole, only the first term in equation (B1) is used, i.e., $\mathbf{u} = \nabla\Phi_P$, and for two-dimensional problems, the third term is not used. The displacement potentials individually satisfy Helmholtz equations and can be expressed in series form as

$$\Phi_P^{(1)} = \sum_{n=-\infty}^{\infty} A_n^P(k_z,\omega)J_n(k_r^{P1}r)e^{i(n\phi+k_z z-\omega t)} , \tag{B5}$$

$$\Phi_P^{(2)} = \sum_{n=-\infty}^{\infty} B_n^P(k_z,\omega)H_n^{(1)}(k_r^{P2}r)e^{i(n\phi+k_z z-\omega t)} , \tag{B6}$$

$$\Phi_{Sh}^{(2)} = \sum_{n=-\infty}^{\infty} B_n^{Sh}(k_z,\omega)H_n^{(1)}(k_r^{S2}r)e^{i(n\phi+k_z z-\omega t)} , \tag{B7}$$

$$\Phi_{Sv}^{(2)} = \sum_{n=-\infty}^{\infty} a\cdot B_n^{Sv}(k_z,\omega)H_n^{(1)}(k_r^{S2}r)e^{i(n\phi+k_z z-\omega t)} , \tag{B8}$$

for three-dimensional problems. The radius of the borehole, *a*, is included in equation (B8) to match the dimension of the coefficients. The superscripts $^{(1)}$ and $^{(2)}$ on the potentials denote (1)=within borehole, and (2)=outside the borehole, which should not be confused with the superscripts on the Bessel (Hankel) functions. Also, the superscripts P1, P2, and S2 indicate P waves inside and outside the borehole, and S wave outside the borehole, respectively. k_r^{P1}, k_r^{P2}, and k_r^{S2} are the radial components of the wavenumbers. It is noted that, since the wavefield

within the borehole is regular and the field outside the borehole is unbounded, Bessel functions of the first kind and Hankel functions for the first kind are used for inside and outside of the borehole, respectively.

For the 2D problem with the physical source, the above equations become

$$\Phi_P^{(1)} = \sum_{n=-\infty}^{\infty} \left[A_n^{P+}(\omega) H_n^{(1)}(k_{P1} r) + A_n^{P-}(\omega) H_n^{(2)}(k_{P1} r) \right] e^{i(n\phi - \omega t)} , \tag{B9}$$

$$\Phi_P^{(2)} = \sum_{n=-\infty}^{\infty} B_n^{P}(k_z, \omega) H_n^{(1)}(k_{P2} r) e^{i(n\phi - \omega t)} , \tag{B10}$$

$$\Phi_{Sh}^{(2)} = \sum_{n=-\infty}^{\infty} B_n^{Sh}(k_z, \omega) H_n^{(1)}(k_{S2} r) e^{i(n\phi - \omega t)} , \tag{B11}$$

where $k_{P1} \equiv \omega / c_{P1}$, $k_{P2} \equiv \omega / c_{P2}$, and $k_{S2} \equiv \omega / c_{S2}$. In this case, since the wavefiled within the borehole fluid is bounded by both borehole wall and the source surface, both kinds of Hankel functions were used in equation (B9).

The stress components are obtained by first computing strain components from equations .(B2), (B3), and (B4), and then applying the Hooke's law to the strains.

REFERENCES

Biot, M.A., 1952, Propagation of elastic waves in a cylindrical bore containing a fluid: J. Appl. Phys., **23**, 997-1009.

Chen, S.T. and E.A. Eriksen, 1991, Compressional and shear-wave logging in open and cased holes using multipole tool: Geophysics, **56**, 550-557.

Cole, J.E., III, 1995, Multipole hydrophone, in Acoustic Particle Velocity Sensors: Design, Performance, and Applications, eds. M.J. Berliner and J. F. Lindberg.

Cole, J.H., 1997, The orbital vibrator, a new tool for characterizing interwell reservoir space, The Leading Edge, March, 281-283.

Daley, T.M. and D. Cox, 2001, Orbital vibrator seismic source for simultaneous P- and S-wave crosswell acquisition: Geophysics, **66**, 1471-1480.

Dong, W., 1994, Elastic wave radiation from borehole seismic sources in anisotropic media, Ph.D. Dissertation, Massachusetts Institute of Technology, 207-226.

Dong, W, 1995, A mathematical model for the downhole orbital vibrator source: 64 th Annual International Meeting, Expanded Abstracts, 90-93.

Dong, W., M. Bouchon, and M.N. Toksoz, 1995, Borehole seismic-source radiation in layered isotropic and anisotropic media: Boundary element modeling: Geophysics, **60**, 735-747.

Hardage, B.A., 1992, Crosswell Seismology and Reverse VSP, Geophysical Press LTD., London, 72-77.

Kurkjian, A.L. and S.K. Chang, 1986, Acoustic mutipole sources in fluid-filled boreholes: Geophysics, **51**, 148-163.

Lee, M.W. and A. H. Balch, 1982, Theoretical seismic wave radiation form a fluid-filled borehole: Geophysics, **47**, 1308-1314.

Liu, E., S. Crampin, and J.H. Queen, 1991, Fracture detection using crosshole surveys and reverse vertical seismic profiles at the Conoco Bohole Test Facililty, Oklahoma: Geophys. J. Int., **107**, 449-463.

Liu, E., J.H. Queen, and Cox, V.D., 2000, Anisotropy and attenuation of corsshole channel waves from the Antrim Shale gas play, Michigan Basin: J. Appl. Geophys., **44**, 47-61.

Nakagawa, S., T.M. Daley, and E.L. Majer, 2003, Waves generated by borehole orbital vibrator source: 73 rd Annual International Meeting, Expanded Abstracts, 2247-2250.

Novascone, S.R., M. J. Anderson, D.M. Weinberg, and J. H. Cole, 2002, Driving point impedance and physical property loggig: 72 nd Annual International Meeting, Expanded Abstracts, abstract in CD-ROM.

Paillet, F.L. and J.E. White, 1982, Acoustic modes of propagation in the borehole and their relationship to rock properties: Geophysics, **47**, 1215-1128.

Van Schaack, M., Harris, J. M., Rector III, J. W., and Lazaratos, S. K., 1995, High-resolution crosswell imaging of a West Texas carbonate reservoir: Part 2- Wavefield modeling and analysis: Geophysics, 60, 682-691.